Real-Time Testing of a Fuzzy Logic Controller Based Grid-Connected Photovoltaic Inverter System

M A Hannan[a], Z A Ghani[a], A Mohamed[a] and M. N. Uddin[c]

[a]Department of Electrical, Electronic & Systems Engineering
Universiti Kebangsaan Malaysia, 43600 Bangi, Selangor, Malaysia
[c]Department of Electrical Engineering, Lakehead University
Thunder Bay, Ontario P7B 5E1, Canada
hannan@eng.ukm.my; zamre@utem.edu.my; azah@eng.ukm.my, muddin@lakeheadu.ca

Abstract –**This paper presents a novel fuzzy logic controller (FLC) based high performance control of a 3-phase photovoltaic (PV) inverter connected to the grid line. For the proposed control scheme one FLC is used for voltage control and two FLCs are used for current controls. With the aid of the developed inverter model and fuzzy voltage and current control schemes, the digital signal processing (DSP) controller board generates the sinusoidal pulse-width modulated (SPWM) logic signals for the inverter operation which regulates the 50 Hz sinusoidal ac output voltage and current for both standalone and grid-connected modes. A prototype PV grid connected 3-phase inverter controlled with the proposed FLCs is built using the DSP board DS 1104. The proposed fuzzy control strategy demonstrates stable ac output voltage of the inverter satisfactorily during both transient and steady-state conditions including grid and/or load disturbances. Moreover, the inverter is capable of feeding excess power to the grid when the power generation is more than local demand. The developed control system generates only 2.48% and 4.64% of output voltage and current total harmonic distortion (THD), respectively. The output waveform results such as the inverter output voltage, injected current, and the system power flow are presented to validate the effectiveness of the control system.**

Keywords - Real-time testing; 3-phase inverter; fuzzy logic controller; voltage control; current control; grid-connected photovoltaic system.

Nomenclature:
R_s internal resistance of stack
I_c output current of the solar cell
I_{ph} light generated cell current
I_o diode reverse saturation current
I_{sat} diode saturated current
T_c cell temperature in Kelvin
A ideality factor
K Boltzmann constant
q electron charge
G irradiance
β voltage temperature coefficient
N_s modules number in series
N_p modules number in parallel
α current temperature coefficient
I_{pv} output current of the PV array
P_{pv} output power of the PV array
T stack temperature
V_{ref} PV reference voltage
I_{ref} PV reference current
T_{ref} reference stack temperature

I. INTRODUCTION

Solar photovoltaic (PV) system has been becoming one of the important renewable energy sources due to its availability and easy access. Since it is a dc power source, an inverter is necessary to convert it to ac power, which can be used to power up ac loads or can be transported to the utility grid [1]. In addition, with proper energy management, the PV power system has become valuable and significant especially, for remote area users, where the utility is unavailable [2]. The success of the PV power utilization is associated with proper control techniques of the inverter [3]. Researchers have been focusing on various inverter control issues including self-consumption losses [4], nonlinearity behavior, output fluctuation, weather dependency and low efficiency of PV [5], electromagnetic interference, harmonics distortion level [6], dc bus voltage fluctuations [7], and attainment of unity power factor [8]. Thus, the design of the inverter controller is a crucial issue for the overall PV system performance [9]-[13]. For easier implementation researchers utilized various types of proportional-integral (PI), and proportional-integral-derivative (PID) controllers to control the PV inverter [14]. However, the well-known disadvantages of the conventional PI, PID controllers and their adaptive versions encourage researchers to apply the intelligent controllers such fuzzy logic, neural network, neuro-fuzzy, genetic algorithm, etc. for PV inverter system [15]-[19]. The main advantages of intelligent controllers are: their designs do not need the exact mathematical model of the system and theoretically they are capable of handling any nonlinearity of arbitrary complexity. Thus, the intelligent controllers are perfect candidate for controlling PV inverter system as the Sun, which is the main source for PV system is unpredictable.

Among the various intelligent controllers fuzzy logic controller (FLC) is the simplest for inverter control. The FLC is better than the conventional controllers in terms of insensitivity to parameter and load variations, response time, settling time and robustness [20]. Table-I presents the summary of inverters system parameters in terms of the output voltage and current harmonics contents, power factor, topology, switching method, implementation, system

978-1-4799-2288-8/14/$31.00 © 2014 IEEE

environment or platform, and utilization of transformers.

Table-I: Summary of inverters parameters in relation to references

Inverter Parameters	Ref. 6	Ref. 9	Ref. 10	Ref. 11	Ref. 12	Ref.13	Ref. 22
Voltage THD	N/A	N/A	N/A	N/A	6.8%	N/A	1.5%
Current THD	6.8	4.0	8.4	8.87	N/A	19.8	N/A
Power Factor	N/A	N/A	0.96	0.994	unity	unity	N/A
Topology	3-Ø 3-L	3-Ø 3-L	1-Ø 5-L	3-Ø 3-L	1-Ø 5-L	3-Ø 3-L	3-Ø 3-L
Switching Technology	PWM	SVPWM	SPWM	SPWM	SPWM	SPWM	PWM
Hardware	Simple	mod	mod	mod	complex	complex	complex
System	Progm	Progm / Simulink	Progm	Progm	Progm	Progm	Progm
Transformer	Yes	no	no	no	no	no	no

* N/A- not available, L-level, mod -moderate, Progm -programming

Apparently, the design of inverters without the transformers seems to be more favorable as it improves the overall inverter physical size and weight [21]. The level of difficulties on the system implementation is associated with the inverter topology, switching topology, and system environment or platform. In regard to the topology and control algorithm, two or three-level type of inverters are simple to be implemented. Multilevel inverters, i.e. above five levels, require a complex control algorithm especially, in switching signals generation and system coordination which adds computational burden to the processor [22]. Moreover, the increased number of semiconductor switches causes the overall system costly [23].

Therefore, in this paper a new fuzzy logic control strategy is developed for high performance control of grid-connected 3-phase photovoltaic inverter system. In order to a test the effectiveness of the proposed control technique a 3 kW prototype PV grid connected 3-phase inverter is built using the DSP board DS 1104. The proposed FLC demonstrates stable ac output voltage of the inverter satisfactorily during both transient and steady-state conditions including the grid and/or load disturbances. Moreover, the inverter is capable of feeding excess power to the grid when the power generation is more than local demand. The developed control system generates only 2.48% and 4.64% of output voltage and current total harmonic distortion (THD), respectively. The output waveform results such as the inverter output voltage, injected current, and the system power flow are presented to validate the effectiveness of the control system. The developed FLC control system also exhibits better performance in reducing the output voltage and current overshoots as compared to the PI controller.

II. PV Based Grid Connected Inverter System

The configuration of the PV based 3-phase grid-connected voltage-source inverter (VSI) system considered in this work is illustrated in Fig. 1.

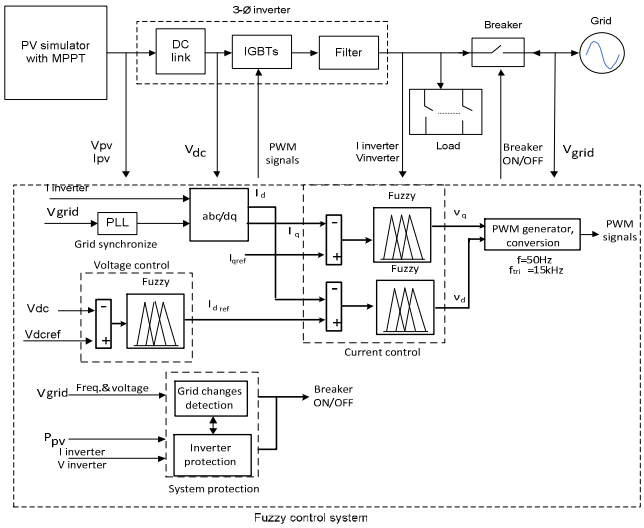

Fig. 1. Overall control scheme for PV based inverter system.

It consists of an FLC control system, PV simulator, inverter and load. The control system consists of several sub-control modules which include voltage and current control functions, grid synchronization, pulse width modulated (PWM) signal generator, abnormal voltage detections such as over and under voltage and frequency. By means of the output parameters sampling such as voltage and current, and implementation of control algorithm, the system controller managed to transfer the maximum PV power to the load as well as stabilizes the ac output voltage, current, and frequency to the desired levels. These objectives are accomplished with the generation of PWM signals for the inverter switching devices. A controllable breaker is used for connecting and disconnecting the inverter to the grid line.

The PV simulator with a built-in dc-dc boost converter and maximum power point tracking (MPPT) algorithm generates the suitable and regulated dc power required by the inverter. The block diagram of the PV simulator is shown in Fig. 2. With the MPPT feature, the PV system transfers maximum power at different solar irradiations. The PV output parameters vary at different solar irradiations and temperature. In this work, for simplification, the implementation is executed only at a fixed solar irradiation of 1000 Watt/m^2 at 25ºC. The parameters of the PV module includes the open circuit voltage, V_{oc} (21.8 V), short circuit current, I_{sc} (5 A), voltage at maximum power, V_{mp} (17 V), and current at maximum power, I_{mp} (4.7 A). The PV array is formed by modules connected in series-parallel combinations to produce total dc output voltage of 408 V with a power capacity of 5.8 kW to be fed to the dc-dc boost converter. In principle, the output voltage of the solar cell is a function of the photocurrent that depends on the solar irradiation level during its operation. The output current of the solar cell can be represented as:

978-1-4799-2288-8/14/$31.00 © 2014 IEEE

$$I_c = I_{ph} - I_o = I_{ph} - I_{sat}\left[e^{\frac{q}{AKT_c}(V+IR_S)} - 1 \right] \quad (1)$$

The voltage and current generated by the PV system depend on the combination of N_s (number of series module) and N_p (number of parallel branch) of PV arrays, which are given by (2) and (3), respectively.

$$V_{PV} = N_S(V_{ref} - \beta(T - T_{ref}) - R_s \quad (2)$$

$$I_{PV} = N_P\left(I_{ref} + \alpha\left(\frac{G}{1000}\right)(T - T_{ref}) + \left(\frac{G}{1000} - 1\right) I_{sc} \right) \quad (3)$$

The power output of the PV array is given by [24]:

$$P_{PV} = I_{PV} \times V_{PV} \quad (4)$$

By utilizing the dc-dc boost converter, the PV voltage, V_{pv} is stepped-up to 700 V for the inverter dc input voltage, V_{dc}. This is achieved by varying the duty cycle, D of the power device using the PWM method, as describe in (5).

$$V_{dc} = \frac{V_{PV}}{1 - D} \quad (5)$$

The topology of the three-phase inverter is shown in Fig. 2. It consists of mainly a dc link, power stage (IGBT inverter) and filters. The dc link consists of a capacitor which links the dc power to the inverter system. Its high capacitance helps to stabilize the input voltage for the inverter. The inverter is connected to the grid through filter inductors which reduce the high-frequency harmonic components injected to the grid system, without a transformer due to cost and size factor [25]. The PWM logic signals S1, S2, S3, S4, S5, S6 and S7 for the inverter and boost converter switches are generated by the controller based on the inverter output parameters and strategy of control algorithm.

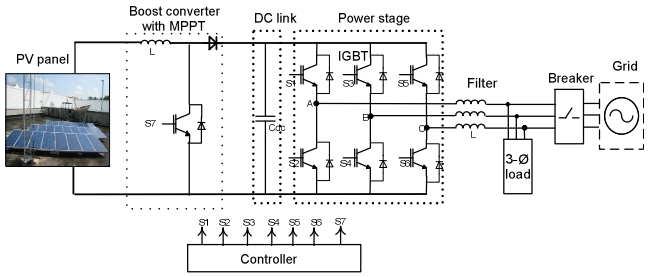

Fig. 2. Three-phase grid-connected inverter topology.

A. Overall Control Principle

The control strategy for the switching signals generation consists of several functional components such as PLL-type grid synchronization, abc-dq0 coordinate transformation, voltage and current regulations, fuzzy-logic controllers, system protections, PWM signals generation and signals conversion.

Initially, in a standalone or off-grid mode, the inverter operates under voltage-controlled scheme and supplies power to the ac loads. The inverter ac output voltage is sensed and converted to *dq0* components by utilizing the Park's transformation. This is to ease the there-phase analysis and design of the control system. Thus, the FLC is able to keep track the reference voltage in both transient and steady-state condition, stabilizing the inverter output voltage and frequency. Once achieved synchronization with the grid, the controllable breaker connects the system to the grid. This is the current-controlled scheme, where the current is controlled and injected to the grid. The FLC tracks the desired current based on the error generated between the actual current components, I_d and I_q, and their respective reference currents, I_{dref} and I_{qref}, which are generated previously in the voltage-controlled scheme. In this scheme, V_{dc} is compared to the reference voltage, V_{dcref} and an error is produced. This error is fed to the FLC for the error minimization. The output signal of the controller serves as a reference current, I_{dref} for the previously described current-controlled scheme.

The other part of the control system is the system protection algorithm. The operability is tested with the application the grid disturbances to the system, e.g. overvoltage, under voltage, over frequency and under frequency. Considering safety as the priority, the breaker contactor opens-up and the inverter shuts down in the present of abnormalities. e.g. grid voltage increase and decrease above 110% and 88% respectively, frequency increase and decrease above 51 Hz and 49 Hz respectively.

III. Proposed Fuzzy Logic Control

The basic architecture of the FLC used in the control strategy is shown in Fig. 3. The main elements that makes up a FLC system are the *fuzzifier* unit at the input terminal, knowledge based (rule base) and the inference engine, and *defuzzifier* at the output terminal. In FLC-based control system, the required variables are the input and output variables. The inputs to the FLC are the parameters or variables of the process to be controlled which depend on the applications. Normally an error and its rate of change are chosen for the input variables. Meanwhile, the change of current and voltage are selected to be the output variables. An error in discrete time is the difference between the desired output or reference, *r(k)*, and the process output variable, *y(k)*. The current sample of error, *e(k)* and the change of error *Δe(k)* are defined in (6) and (7), respectively.

These variables universal discourse, which are normalized to fit into the interval value between -1 and +1, acquire seven membership functions as shown in Fig. 4. For simplification, the triangular and trapezoidal membership functions are used. The membership functions are labeled as NB for 'Negative Big', NM for 'Negative Medium', NS for 'Negative Small', ZE for 'Zero', PS for 'Positive Small', PM for 'Positive Medium' and PB for 'Positive Big'. The input variables are fuzzified through these membership functions.

978-1-4799-2288-8/14/$31.00 © 2014 IEEE

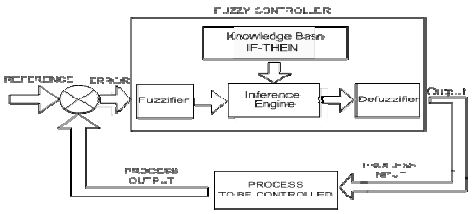

Fig. 3. Fuzzy logic control architecture.

$$e(k) = r(k) - y(k) \tag{6}$$

$$\Delta e(k) = e(k) - e(k-1) \tag{7}$$

By the essence of the inference process and with the aid of the knowledge-based rules, the fuzzy output is generated. The important part of the FLC is the knowledge-based element, which consists of a list of fuzzy rules [27]. The inference process is to generate a fuzzy output set according to the IF-THEN rules base. With these rules, the fuzzy controller behaves intelligently and capable of imitating humanlike-decision. There are 49 rules of 'IF-THEN' logic related to the inputs and outputs as shown in Fig. 4. This logic makes the control function into a FLC. From the figure, some of the rules are as follows:

Rule 1: IF 'error (e)' is NB AND 'Δerror (Δe)' is NB THEN Δu is NB
Rule 2: IF 'error' is NM AND 'Δerror' is NB THEN Δu is NB
Rule 3: IF 'error' is NS AND 'Δerror' is NB THEN Δu is NM
Rule 4: IF 'error' is ZE AND 'Δerror' is NB THEN Δu is NM
Rule 5: IF 'error' is PS AND 'Δerror' is NB THEN Δu is NS
- -
Rule 49: IF 'error' is PB AND 'Δerror' is PB THEN Δu is PB

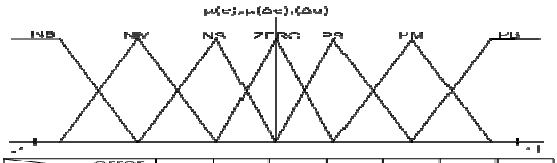

Δerror \ error	NB	NM	NS	ZE	PS	PM	PB
NB	NB	NB	NM	NM	NS	ZE	ZE
NM	NB	NM	NM	NS	NS	ZE	PS
NS	NM	NM	NS	NS	ZE	PS	PS
ZE	NM	NS	NS	ZE	PS	PS	PM
PS	NS	NS	ZE	PS	PS	PM	PM
PM	NS	ZE	PS	PS	PM	PM	PB
PB	ZE	PS	PS	PM	PM	PB	PB

Fig. 4. Membership functions for error, change of error, controller output and rule based matrix table.

In the system implementation, the fuzzy controller output, $u(k+1)T_s$, keep changing in every sampling time until it reaches a steady-state condition as described in (7) [27].

$$u(k+1) = u(k) + \Delta u(k) \tag{8}$$

where, $\Delta u(k)$ is the sample of controller output. In this work, the center of area *defuzzification* method is used to calculate the actual output from its fuzzy value as given in (8).

$$u = \frac{\sum_{i=1}^{k} u_i \times \mu(u_i)}{\sum_{i=1}^{k} \mu(\mu_i)} \tag{8}$$

where $\mu(u_i)$ is membership value of the combined membership function.

IV. DSP BASED PROTOTYPE IMPLEMENTATION

In order to validate the effectiveness of the proposed algorithms in real-time the proposed FLC based PV grid connected inverter system is experimentally implemented using dSPACE DSP board DS1104 [28]. The experimental test set up for the prototype PV based grid connected 3-phase inverter is shown in Fig. 5. The DSP board DS1104 is installed inside a personal computer with uninterrupted communication capability through a dual port memory. The DS1104 board is mainly based on a 64-bit PowerPC type PPC603e processor. The DSP is supplemented by a set of on-board peripherals used in digital control systems including analog to digital (A/D), digital to analog (D/A) converters and digital incremental encoder interfaces.

For real-time implementation, a real-time Simulink model is developed and then downloaded to the DSP board utilizing using the MATLAB/Simulink real-time workshop (RTW) tool and dSPACE ControlDesk software. With the application of the dSPACE graphical user interface (GUI) software, the monitoring of the performance and behavior of the inverter in real time is made possible. Moreover, the user is able to alter the controller parameters and immediately observe the effect of the system performance in real time as well.

Fig. 5. Test set-up for prototype PV based grid-connected inverter system.

V. RESULTS AND DISCUSSION

The prototype implementation of the developed inverter control system was tested by downloading the real-time simulation model into DSP board utilizing MATLAB real-time RTW tool and dSPACE control software. Fig. 6 shows the tested waveforms of inverter output voltage, injected current and grid voltage for one phase for a period of 0.16 s with a sampling period of 5 μs.

978-1-4799-2288-8/14/$31.00 © 2014 IEEE

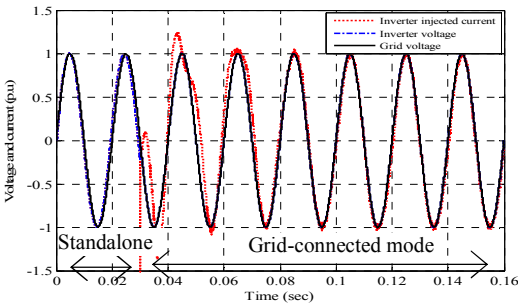

Fig. 6. Inverter injected current, inverter voltage and grid voltage.

It is seen from this figure that all the waveforms are nearly sinusoidal with a frequency of 50 Hz and having peak voltages of 1.0 p.u. This is equivalent to rms phase voltage of 240 V or line voltage of 415 V. Initially, the system is started in a standalone mode operating as a voltage- controlled inverter. Then, the inverter acquires the grid frequency and phase, thus make it possible to connect to the grid. Once synchronized, the grid-connecting switch is closed and the system operated in a grid-connected mode and behaved as a current-controlled inverter at 0.03 s. This is an important feature that a PV grid-connected inverter should acquire in order to connect to the grid safely. It can be seen that the voltage is kept constant during the period of connection with the grid, as to provide constant power flow to the grid. The injected current achieved in-phase condition with the grid voltage (unity power factor) except at the beginning of the connection due to some control algorithm delay. During the grid-connected mode, the system operated in current-control scheme and the behavior of the reference-current tracking can be seen with very small ripples in the current waveform. The role of the FLC in regulating the injected current to the grid was depicted by the constant level of the current waveform. In other words, the inverter was able to transfer the constant PV power to the grid and load.

It is important to know the power flow of the PV grid-connected inverter system. The inverter system power flow is shown in Fig. 7.

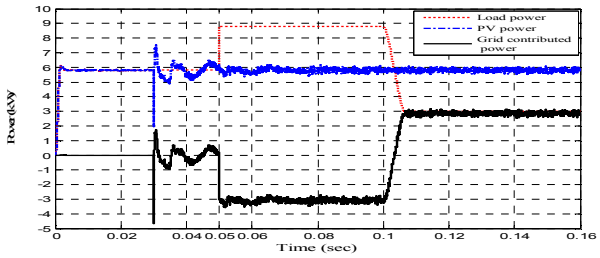

Fig. 7. System power flow.

For the period of 0 to 0.05 s, the load demand is 5.8kW which considered as 100% load scenario, there is almost no power flowing to the grid. This is due to a power balance condition between PV and load, where the generated power is equal to the power demand. During the grid-connected mode, from 0.05 to 0.1 sec., the load power is increased to 8.8 kW. This is considered as 150% load scenario which is equivalent to an increase of 3 kW. This is a condition where the load demands more power from the PV. Since PV has the capacity of 5.8 kW, the additional balance of power is drawn from the grid which is indicated by -3 kW in the grid contribution profile in the figure. The grid continues to supply power to the load until 0.1 sec., when the load is reduced to 3.0 kW. This is a 50% load scenario, where the load uses less power compared to the generated one. Hence, the excess power from the PV which is approximately 3 kW is dispatched to the grid which shown by the + 3.0 kW in grid contribution profile line. The analysis of power flow scenarios has demonstrated the ability of the inverter to extract power from the PV and feed to the load and grid.

The load voltage and current waveforms during the load demand variations are presented in Fig. 8.

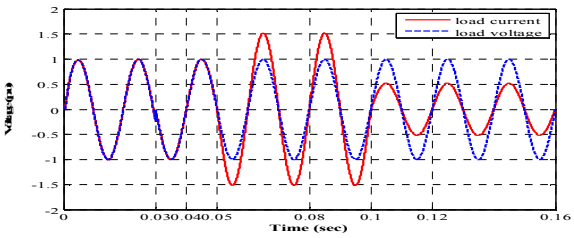

Fig. 8. Load voltage and current waveforms during load demand variation.

Both waveforms are in phase during the load variations period. An increased of the load power demand beyond the PV capacity has caused the additional power drawn from the grid. This is shown by the current waveform during the period of 0.05 to 0.1 s. A drop of load power demand after 0.1 s onward has shown a decreasing of load current. Consequently, the excess of PV power was exported to the grid. Importantly, the load voltage was kept constant regardless of the load power profile as to provide constant power flow to the load and grid.

The criterion of having quality output power acquiring lower voltage and current harmonic contents for the inverter is important especially when connecting to the grid. By utilizing the Fast-Fourier transform (FFT) technique, the THD of the phase voltage and current waveforms are calculated to be 2.48% and 4.64% respectively. These levels are below 5% and complied with the IEEE Std. 929-2000 [29]. The waveforms and their respective harmonics spectrums are shown in Fig. 9 and Fig. 10.

The harmonic levels are resulted from the effectiveness of the control algorithm that employs the FLC, SPWM technique, voltage and current-controlled algorithms, and filter. The performance of the FLC and PI controller are evaluated in terms of transient and steady-state response in stabilizing the dc link voltage for ensuring low ripple on the inverter ac output waveform.

978-1-4799-2288-8/14/$31.00 © 2014 IEEE

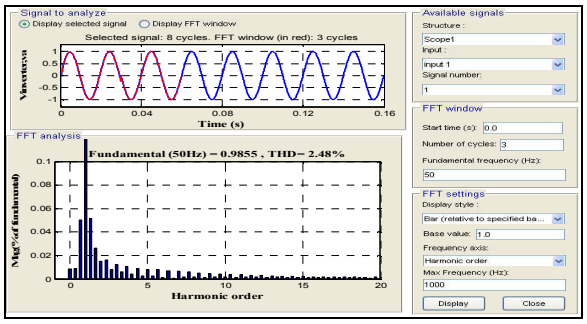

Fig. 9. THD and harmonics spectrum of inverter output voltage

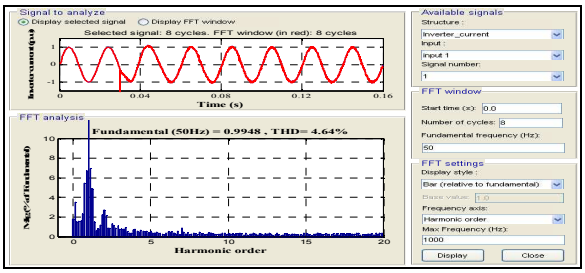

Fig. 10. THD and harmonics spectrum of inverter output current.

During the standalone mode, FLC exhibited good response with no overshoot during the initial stage of the transient response as shown in Fig. 11.

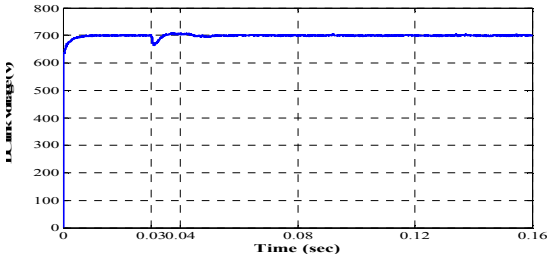

Fig. 11. DC link voltage waveform controlled by FLC.

Unlike the FLC, PI controller transient response shows an overshoot occurred at the starting point before stabilized which can be seen in Fig. 12. The steady-state response characteristic for the grid-connected mode was considered good for both controllers as can be seen after t = 0.04 s onwards.

The inverter behaviors during grid disturbances are shown in the following figures. Such disturbances are purposely applied in order to access to ability of the inverter control algorithm to handle disturbances in a safely and properly manner. The scenarios are overvoltage, under-voltage, over-frequency and under-frequency. Such responses were evaluated based on [28] which stated that the inverter should cease to energize the utility line in the conditions where the grid voltage increased above 110% (264 V) and dropped below 88% (211 V) of the nominal voltage, 240 V. As for the frequency, the inverter system was evaluated for the frequency increased above 51 Hz and decreased below 49 Hz. The disturbances were introduced for a time period of 0.06 to 0.095 s. The results of the systems were shown and described in the following text.

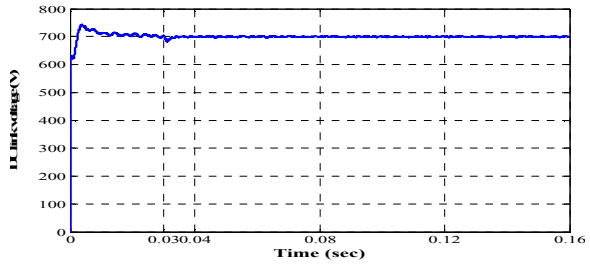

Fig. 12. DC link voltage waveform controlled by PI

Fig. 13 shows the over frequency situation when the grid frequency was increased to 51 Hz.

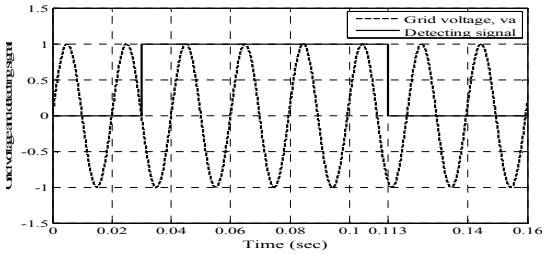

Fig. 13. Grid voltage and detecting signal during frequency increase

Initially, the inverter was in a standalone mode which shown by the zero grid current. Then at 0.03 sec. it connected to the grid. After detecting the disturbance which occurred from 0.06 to 0.09 sec., the inverter disconnected itself from the grid, and then shut down at 0.113 sec. The isolation process, which is the moment of the disturbance occurrence to the time of grid disconnection, was approximately 2.65 cycles. It complies with the requirement of IEEE Std. 929-2000. This can be seen in Fig. 14, where at 0.113 sec. onward, the inverter voltage and grid supplied current were zero, resulted from the inverter shutting down and grid-isolating algorithm, as to provide safety protections.

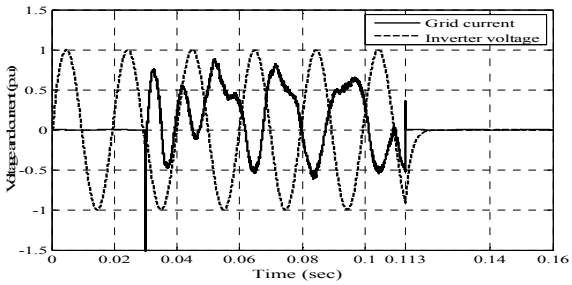

Fig. 14. Grid current and inverter voltage for grid frequency increase

The under frequency scenario when the grid frequency dropped to 49 Hz is shown in Fig. 15.

978-1-4799-2288-8/14/$31.00 © 2014 IEEE

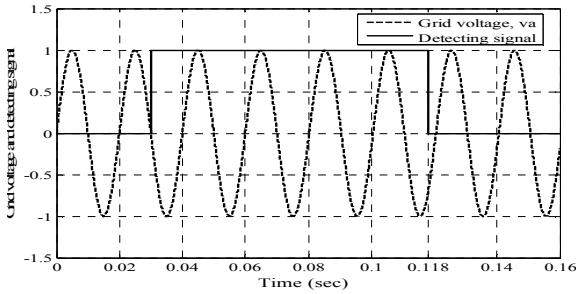

Fig. 15.Grid voltage and detecting signal during frequency decrease

The inverter started with the standalone mode, operating with zero grid current, and then connected to the grid at 0.03 sec. The inverter has detected the disturbance which occurred at 0.065 sec., and then turned off and isolated itself from the grid at 0.118 sec. Like the over frequency case, the inverter shutting down and isolating process took about 2.65 cycles which is within the range of the IEEE requirement. As important as in the over frequency scenario, the under frequency disturbance occurrence should be managed so that device and personnel protection are guaranteed. This can be seen from Fig.16 where at 0.118 sec. onward, the inverter voltage and grid supplied current were zero, owing to the inverter shutting down and grid-isolating algorithm.

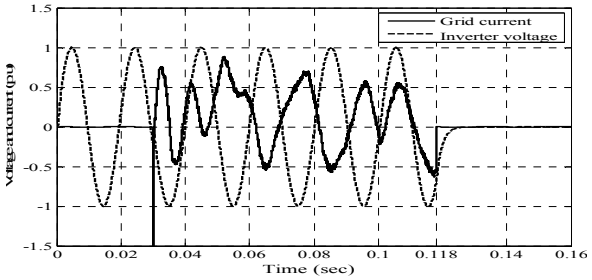

Fig. 16. Grid current and inverter voltage for grid frequency decrease

Fig. 17 shows the inverter reaction when detecting grid voltage increase to 264 V.

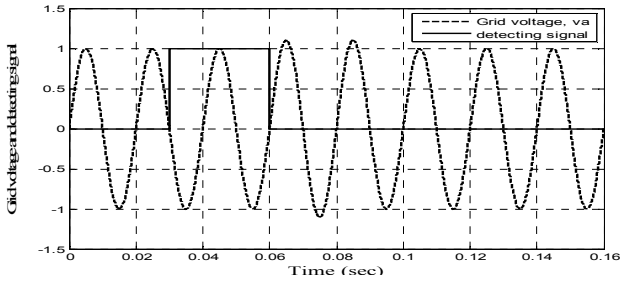

Fig. 17. Detecting signal for grid voltage increase

Initially, the inverter operated in standalone mode and then started to connect to the grid at 0.03 sec. This is shown by the 'high' voltage level of the detecting signal. The inverter has detected the grid over voltage disturbance which occurred at 0.06 sec., and then caused the detecting signal to become 'low' level, disconnecting it from the grid and switched off the inverter simultaneously. Consequently, there was no grid current flowing through and the inverter terminal voltage became zero as in Fig. 18.

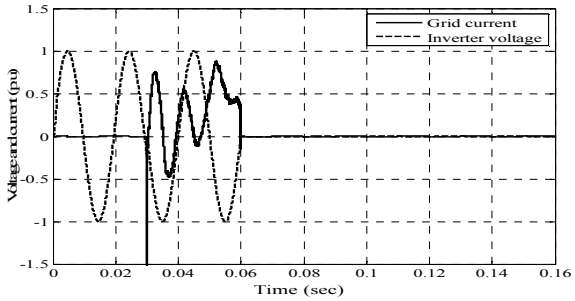

Fig. 18. Grid current and inverter voltage during grid voltage increase

The inverter behavior when the grid voltage dropped to 211 $V_{rms}$is shown in Fig. 19.

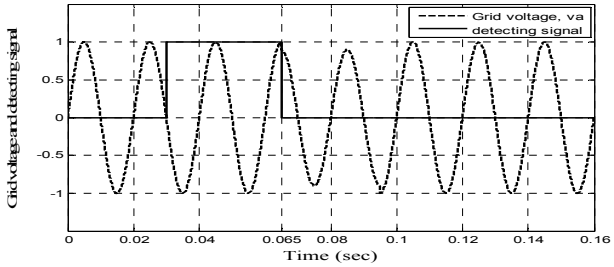

Fig. 19. Inverter voltage and grid current for grid voltage decrease

Initially, the inverter was in standalone mode and then started to connect to the grid at 0.03 sec. This is shown by the 'high' voltage level of the detecting signal. The grid under voltage disturbance was set at 0.065 sec. Upon detection, the control system has caused the detecting signal to become 'low' level, isolating it from the grid and immediately switched off the inverter. As a result, no grid current flowing through and the inverter terminal voltage became zero as in Fig. 20.

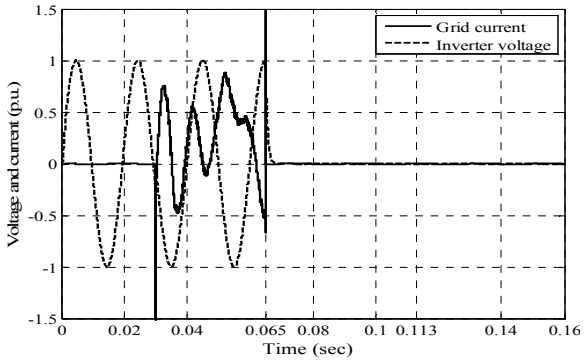

Fig. 20. Grid current and inverter voltage during grid voltage decrease

978-1-4799-2288-8/14/$31.00 © 2014 IEEE

VI. CONCLUSION

The developed model for the grid-connected 3-phase PV inverter and the control system for the prototype realization have been presented. The control algorithm was implemented in DSP board utilizing MATLAB/Simulink with three different load scenarios and the grid voltage and frequency disturbance scenarios. The presented results showed that the inverter control system employing FLC is very effective in producing stable and nearly 50 Hz sinusoidal waveform both voltage and current. Moreover, the inverter is able to transfer the available PV power to the utility grid. Besides, the inverter has successfully detected the occurrences of grid disturbances and capable of disconnecting it from the grid as to provide protection for both device and personnel. Compare to the overall inverter system implementation presented in Table1, the proposed fuzzy controlled inverter is better in terms of the generating quality PV power to the grid, unity power factor, system implementation and computation burden. Thus, suggesting that the developed control system is very effective and practical for the prototype realization utilizing dSPACE DS1104 controller.

Acknowledgement- The authors acknowledge the financial support received under the grant DPP-2014-143 and 06-01-02-SF1060.

REFERENCES

[1] A. Zahedi, "A Review of Drivers, Benefits, and Challenges in Integrating Renewable Energy Sources Into Electricity Grid,"*Renewable and Sustainable Energy Reviews*,vol. 15, pp. 4775-4779, 2011.

[2] G. Kyriakarakos, A.I. Dounis, K.G. Arvanitis, G. Papadakis, "A fuzzy Logic Energy Management System for Polygeneration Microgrids,"*Renewable Energy*,vol 41, pp. 315-327, 2012.

[3] H. Jiayi, J. Chuanwen, X. Rong, "A Review on Distributed Energy Resources and Microgrid,"*Renewable and Sustainable Energy Reviews*, vol. 12, pp. 2472-2483, 2008.

[4] J. D. Mondol, Y.G. Yohanis, B. Norton, "The Impact of Array Inclination and Orientation on the Performance of a Grid-Connected Photovoltaic System,"*Renewable Energy*,vol. 32, pp. 118-140, 2007.

[5] M. Datta, T. Senjyu, A. Yona, T. Funabashi, "A Fuzzy Based Method for Leveling Output Power Fluctuations of Photovoltaic-Diesel Hybrid Power System,"*Renewable Energy*, vol. 36, pp. 1693-1703, 2011.

[6] F. Botteron, H. Piheiro, "Descrete-Time Internal Model Controller for Three-Phase PWM Inverters With Isolator Transformer, *IEEE Proceeding of Electric Power Application*, vol. 153, pp. 57-67, 2006.

[7] M. A. Hannan, Z. A. Ghani, A. Mohamed, "An Enhanced Inverter Controller for PV Applications Using the dSPACE Platform, *International Journal of Photoenergy*, vol. 2010, pp. 1-10, doi:10.1155/2010.

[8] L. Hassaine, E. Olias, J. Quintero, M. Haddadi, "Digital Power Factor Control and Reactive Power Regulation for Grid-Connected Photovoltaic Inverter," *Renewable Energy*, vol. 34, pp. 315-321, 2009.

[9] M. Sreedevi, P. J. Paul, "Fuzzy PI Controller Based Grid-Connected PV System," *International Journal of Soft Computing*, vol. 6, pp. 11-15, 2011.

[10] A. Hmidet, R. Dhifaoui, O. Hasnaoui, "Development, Implementation and Experimentation on a dSPACE DS1104 of a Direct Voltage Control Scheme," *Journal of Power Electronics*, vol. 10, pp. 468-476, 2010.

[11] S. Alepuz, S. Busquets-Monge, J. Bordonau, J. Gago, D. Gonzalez, J. Balcells, "Interfacing Renewable Energy Sources to the Utility Grid Using a Three-Level Inverter," *IEEE Transactions on Industrial Electronics*, vol.53, pp. 1504-1511, 2006.

[12] N. A. Rahim, J. Selvaraj, C. Krismadinata, "Five-Level Inverter With Dual Reference Modulation Technique for Grid-Connected PV System," *Renewable Energy*, vol. 35, pp. 712–720, 2010.

[13] P. Bhubaneswari, S. Iniyan, G. Ranko, "A Review of Solar Photovoltaic Technologies," *Renewable and Sustainable Energy Reviews*, vol. 15, pp. 1625-1636, 2011.

[14] E. K. Ahmad, N. A. Rahim, J. Selvaraj, "Optimized PID Controller for Both Single Phase Inverter and MPPT SEPIC DC/DC Converter of PV Module," *Proceeding of IEEE International Electric Machines & Drives Conference*, pp. 1036-41, 2011.

[15] C. Cecati, F. Ciancetta, P. Siano, "A Multilevel Inverter for Photovoltaic for Photovoltaic Systems With Fuzzy Logic Control," *IEEE Transaction on Industrial Electronics*, vol. 57, no. 12, pp. 4115-4125, 2010.

[16] D. O. Abdeslam, P. Wira, J. Merckle, D. Flieller, "Artificial Neural Networks to Control an Inverter in a Harmonic Distortion Compensation Scheme," *IEEE International Symposium on Industrial Electronics*, pp. 1879-1884, doi: 10.1109/ISIE.2008.4677022, 2008.

[17] T. Govindaraj, N. M. Dhivya, "Simulation Modelling on Artificial Neural Network Based Voltage Source Inverter Fed PMSM," *International Journal of Innovative Research in Electrical, Electronics, Instrumentation and Control Engineering*, vol. 2, no. 1, pp 785-792, 2014.

[18] N. Altin, I. Sefa, "Simulation of Neuro-Fuzzy Controlled Grid-Connected Inverter," *XXIII International Symposium on Communication and Automation Technologies*, pp.1-7, 27-29 Oct. 2011.

[19] E. Koutroulis, F. Blaabjerg, "Methods for the Optimal Design of Grid-Connected PV Inverters," *International Journal Of Renewable Energy Research*, vol. 1, no. 2, pp 54-64, 2011.

[20] S. Premrudeepreechacharn, T. Poapornsawan,"Fuzzy Logic Control of Predictive Current Control for Grid-Connected Single Phase Inverter," *Twenty-Eighth IEEE Photovoltaic Specialists Conference*, pp. 1715-1718, 2000.

[21] L. Pisit, P. Serge, M.T. Farid, "Nonlinear Control Techniques of a Controllable Rectifier/Inverter-Motor Drive System With a Small DC-Link Capacitor,"*Energy Conversion and Management*, vol. 49, pp. 3541-3549, 2008.

[22] C.L. Poh, G.H. Donald, "Analysis of Multiloop Control Strategies for LC/CL/LCL-Filtered Voltage-Source and Current-Source Inverters,"*IEEE Transaction on Industry Applications*,vol. 41, pp. 644-654, 2005.

[23] L. Shuhui, T.A. Haskew, L. Dawen, H. Fei, "Integrating Photovoltaic and Power Converter Characteristics for Energy Extraction Study of Solar PV Systems,"*Renewable Energy*, vol. 36, pp. 3238-3245, 2011.

[24] P. J. Perez, G. Almonacid, J. Aguilera, J. Casa, "RMS Current of a Photovoltaic Generator in Grid-Connected PV Systems: Defination and Application," *International Journal of Photoenergy*, vol. 2008, pp. 1-8, doi:10.1155/2008/356261.

[25] K. Bandara, T. Sweet, J. Ekanayake, "Photovoltaic Applications for Off-Grid Electrification Using Novel Multi-Level Inverter Technology With Energy Storage," *Renewable Energy*, vol. 37, pp. 82-88, 2012.

[26] D.K. Chaturvedi, *Modeling and Simulation of Systems Using MATLAB and Simulink*, CRC Press, 2006.

[27] Z. Kovacic, S. Bogdan, *Fuzzy Controller Design: Theory and Applications*, CRC Press, 2006.

[28] dSPACE DS1104, *Hardware Installation and Configuration and ControlDesk Experiment Guide*, Paderborn, Germany, 2008.

[29] IEEE Std 929-2000. *Recommended Practices for Utility Interface of Photovoltaic System*, The Institute of Electrical and Electronics Engineers, New York, 2002.

978-1-4799-2288-8/14/$31.00 © 2014 IEEE